



저작자표시-비영리-변경금지 2.0 대한민국

이용자는 아래의 조건을 따르는 경우에 한하여 자유롭게

- 이 저작물을 복제, 배포, 전송, 전시, 공연 및 방송할 수 있습니다.

다음과 같은 조건을 따라야 합니다:



저작자표시. 귀하는 원저작자를 표시하여야 합니다.



비영리. 귀하는 이 저작물을 영리 목적으로 이용할 수 없습니다.



변경금지. 귀하는 이 저작물을 개작, 변형 또는 가공할 수 없습니다.

- 귀하는, 이 저작물의 재이용이나 배포의 경우, 이 저작물에 적용된 이용허락조건을 명확하게 나타내어야 합니다.
- 저작권자로부터 별도의 허가를 받으면 이러한 조건들은 적용되지 않습니다.

저작권법에 따른 이용자의 권리는 위의 내용에 의하여 영향을 받지 않습니다.

이것은 [이용허락규약\(Legal Code\)](#)을 이해하기 쉽게 요약한 것입니다.

[Disclaimer](#)

Distinct Climate Response to Radiative Cooling Over North Asia and North America

Jiyeong Kim

Department of Urban and Environmental Engineering
(Environmental Science and Engineering)

Graduate School of UNIST

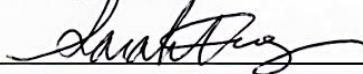
Distinct Climate Response to Radiative Cooling Over North Asia and North America

A thesis/dissertation
submitted to the Graduate School of UNIST
in partial fulfillment of the
requirements for the degree of
Master of Science

Jiyeong Kim

12/18/2019

Approved by



Advisor

Sarah Kang

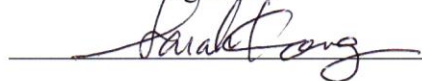
Distinct Climate Response to Radiative Cooling Over North Asia and North America

Jiyeong Kim

This certifies that the thesis/dissertation of Jiyeong Kim is approved.

12/18/2019

signature



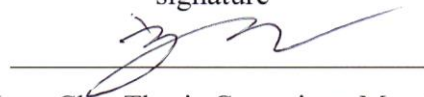
Advisor: Sarah Kang

signature



Myong-In Lee: Thesis Committee Member #1

signature



Dong-Hyun Cha: Thesis Committee Member #2

Abstract

We contrast the patterns of tropical climate response to localized radiative cooling forcing over different two continents in an atmospheric model coupled to a slab ocean and a fully coupled model with an ocean dynamics. Without ocean dynamics, atmospheric heat transport compensates most of the forcing. The slab ocean model produces similar patterns of tropical climate responses that are nearly insensitive of the longitudinal forcing location. Common patterns of interhemispheric temperature contrast accompany a southward shift of the Intertropical Convergence Zone. In contrast, the fully coupled model produces distinct spatial distributions of tropical precipitation responses depending on the forcing location. The change of surface pressure pattern affects the climatological northeasterly wind over the tropical Pacific Ocean. It determines the efficiency of ocean circulation components: Wind-driven shallow overturning circulation or Deep overturning circulation. A strengthening of the Atlantic Meridional Overturning Circulation to an imposed North America cooling effectively brings the heat and explains most of the ocean heat transport response. However, Pacific trade winds tend to be weakened in response to anomalous low-pressure over the Northern Pacific Ocean, hence the influence of Indo-Pacific Ocean heat transport is very small. North Asia cooling produces comparable contribution of ocean heat transport in both the Atlantic and Indo-Pacific Ocean. High-pressure anomaly over the Northern Pacific Ocean induces a strengthening of the equatorial Pacific trade winds, the northward Ekman transport, and the subtropical cell in the Northern Hemisphere. It is a major contributor to the experimental difference of ocean compensation, in turn, it causes different patterns of tropical precipitation response.

Contents

I. Introduction -----	1
II. Methods -----	3
2.1 Data, Model and Experiments -----	3
2.2 Analysis Methods -----	5
III. Results -----	8
3.1 Responses of surface temperature and precipitation -----	8
3.2 Atmospheric energy budget and TOA radiation response -----	10
3.3 Ocean heat budget and MOC response -----	13
3.4 Coupling of the atmosphere and ocean circulations -----	15
IV. Conclusion and Discussion -----	17

List of figures

Fig. 2.1.1. Annual mean precipitation (mm/day) and SST (K) from (a, c) the mean of 40 CMIP5 multi-models and (b, d) GFDL AM4-FLOR for pre-industrial control run. PCORR indicates the value of pattern correlation.

Fig. 2.1.2. Distribution of imposed radiative forcing (Wm^{-2}) over North Asia (left) and North America (right).

Fig. 3.1.1. The response of annual mean global surface temperature for (a) SOM-N.Asia, (b) SOM-N.Amer, (c) DOM-N.Asia, and (d) DOM-N.Amer. The black outlined boxes indicate the region with the prescribed forcing.

Fig. 3.1.2. The zonal mean responses of (a) surface temperature (K) and (b) precipitation (mm/day) for DOM cases (solid) and SOM cases (dashed). The blue shading regions indicate latitudinal bands of forcing.

Fig. 3.1.3. The response of annual mean global precipitation (shading) for (a) SOM-N.Asia, (b) SOM-N.Amer, (c) DOM-N.Asia, and (d) DOM-N.Amer. Contours denote the climatological precipitation in the CTRL (contour interval = 3 mm/day). The black outlined boxes indicate the region with the prescribed forcing.

Fig. 3.2.1. The fractional compensation (%) by the atmospheric heat transport (C_{ATM}), the ocean heat uptake (C_{OCN}), and the TOA radiation (C_{TOA}) averaged between 5°S and 5°N for (a) SOM and (b) DOM. The red bar indicates N.Asia case and the blue bar indicates N.Amer case.

Fig. 3.2.2. The response of TOA radiation (shading; Wm^{-2}) and their zonal-mean plots for (a-c) SOM and (d-f) DOM. Contour indicates the low cloud amount response (in %; positive in solid and negative in dashed). Positive denotes downward fluxes for TOA.

Fig. 3.3.1. (a) Changes of net downward surface heat flux averaged between 5°S and 5°N in the total (blue), Eulerian mean OHT (olive), residual OHT (green), and OHS (cyan). (b) The responses of meridional OHT averaged between 5°S and 5°N in the total (olive), the Atlantic Ocean (pink), and the Indo-Pacific Ocean (purple).

Fig. 3.3.2. The annual mean ocean MOC streamfunction responses (shading; in Sv) and mean ocean

MOC in DOM-CTRL (contour interval = 5 Sv) in (a, b) the Atlantic Ocean and (c, d) the Indo-Pacific Ocean. Solid (dashed) contour denotes a clockwise (counterclockwise) circulation.

Fig. 3.4.1. Composite annual mean anomalies of surface winds and sea level pressure for (a) SOM-N.Asia, (b) SOM-N.Amer, (c) DOM-N.Asia, and (d) DOM-N.Amer. The shading indicates the wind speed responses. The green contour indicates the sea level pressure responses (contour interval = 0.25 hPa). Solid (dashed) contour denotes the high (low) pressure anomaly. The vectors indicate the 10m wind anomalies.

I. Introduction

If there is an interhemispheric temperature contrast on Earth, the Hadley circulation plays a crucial role in transporting excessive heat to the cooler hemisphere in the atmosphere. At this time, the upward branch of the Hadley circulation moves towards the warmer hemisphere, resulting in a change in the Intertropical Convergence Zone (ITCZ) (Kang et al. 2008), which is the main feature of the tropical climate. Because the ITCZ accounts for one-third of global precipitation, its shape and location affect not only local variations in rainfall but also global climate responses, such as changing the hurricane frequency (Merlis et al. 2013), the mid-latitude jet position (Ceppi et al. 2013) and hemispheric albedo asymmetry (Voigt et al. 2014). It is therefore important to study how the ITCZ will respond to external forcing.

One might expect that the tropical climate is mainly changed by local perturbation. But, according to paleoclimate data, interhemispheric temperature contrast in the extratropics is strongly correlated with proxies of ITCZ migration (Schneider et al. 2014). In this regard, we recognized that the response in extratropics could affect the ITCZ location. Previous simulations show how extratropical perturbations affect the tropical climate. For example, Chiang and Bitz (2005) find that the changes in prescribed ice coverage lead to the Northern Hemisphere (NH) cooling response, in turn, it induces a clear meridional shift of ITCZ.

Before, most studies about ITCZ response to extratropical forcing have demonstrated using the only atmospheric model even though the real earth has an ocean dynamic. Recently, Kay et al. (2016) show that the impact of ocean dynamics on the ITCZ response, comparing between a fully coupled model and a fixed ocean dynamic model, called a slab ocean model. They reduce insolation over the entire Southern Ocean, then it makes the cooling response and northward ITCZ shift. Because the cross-equatorial atmospheric heat transport (AHT) determines the magnitude of ITCZ shift, larger cross-equatorial AHT in the slab ocean model shows a clear northward ITCZ shift. However, in the fully coupled model, the cross-equatorial AHT is very small due to ocean dynamics, hence it dampens the ITCZ shift. The damping results are consistent with other studies using the fully coupled model (Deser et al. 2015; Green and Marshall 2017; Hawcroft et al. 2017; Xiang et al. 2018).

Several studies with the fully coupled model have addressed the shift of ITCZ to zonally symmetric forcing in different latitudes, focusing on the role of the ocean dynamics (Kay et al. 2016; Hawcroft et al. 2018; Xiang et al. 2018). However, the real perturbation is inhomogeneous in longitude due to aerosol forcing (Allen et al. 2015; Hwang et al. 2013; Westervelt et al. 2018), vegetation (Levis et al. 2004; Notaro et al. 2007), sea ice variations (Chiang and Bitz 2005; Sewall et al. 2004) or land cover changes (Matthews et al. 2003; Feddema et al. 2005). Without ocean dynamics, in Kang et al. (2018), the tropical climate patterns are almost the same regardless of whether the forcing is located in the

Pacific or the Atlantic Ocean. Unlike the results, studies with dynamical ocean note that the change of tropical precipitation largely depends on the detail including the location and shape of perturbation (Westervelt et al. 2018; White et al. 2018).

In particular, the changes in ocean circulation are efficient at transporting heat to the cooler hemisphere through wind-driven shallow overturning circulations (Schneider 2017; Green and Marshall 2017; Kang et al. 2018a) or thermohaline circulations (Fuehrer et al. 2013; Yu and Pritchard 2019; Frierson et al. 2013) such as the Atlantic Meridional Overturning Circulation (AMOC). But, it is not clear how these ocean circulations are associated with localized perturbation.

To show the climate patterns in response to localized perturbation, our simulations are performed with a simplified radiative forcing through the reduction of solar radiation over extratropical North Asia or North America. We focus on the magnitude of zonal-mean tropical climate response, in particular, the partitioning of the energy transport between atmosphere and ocean, and the efficiency of varying ocean circulation components. We also examine the spatial pattern of tropical climate response, and the differences between the slab ocean model and the fully coupled model, which can distinguish the impact of the dynamic ocean. Therefore, we study the dependence of the tropical climate response on the longitude of extratropical perturbation.

II. Methods

2.1 Data, Model and Experiments

2.1.1 Data and Model

We use several observational datasets over the period between 1979 and 2005, including precipitation from the Global Precipitation Climatology Project version 2.2 (GPCP), radiative fluxes from Clouds and the Earth's Radiant Energy System version 2.8 (CERES), and sea ice and sea surface temperature (SST) from the Met Office Hadley Centre Sea Ice and Sea Surface Temperature dataset (HadISST1).

We perform experiments with Geophysical Fluid Dynamics Laboratory (GFDL) Atmospheric Model version 4 (AM4; Zhao et al. 2018) coupled to a dynamic ocean model (DOM) used in GFDL Forecast-Oriented Low Ocean Resolution (FLOR) (Vecchi et al. 2014) and coupled to a 50m slab ocean model (SOM) with realistic topography. The atmospheric model has a horizontal resolution of 1° latitude x 1.25° longitude with 32 vertical levels. The oceanic model has an approximate horizontal grid spacing of 1° with 50 vertical levels. We compare our model control precipitation and SST with 40 CMIP5 multi-model mean shown as Figure 2.1.1. We use the pre-industrial period for control simulation. The spatial patterns of precipitation and SST are qualitatively equivalent to the CMIP5 multi-model means, which has very high pattern correlations of more than 0.95.

2.1.2 Experiments

A fully coupled control simulation runs for 200 years after 500 years of spin-up (DOM-CTRL) as described by Xiang et al. (2018), and the control run for the SOM is spun up and integrated for 100 years (SOM-CTRL). The atmosphere composition such as greenhouse gases and aerosols are forced by the year 2000 conditions.

Perturbed runs are starting from the same initial condition as CTRL run. To examine whether results are sensitive to the longitudinal location of perturbation, we prescribe localized forcing with top-of-the-atmosphere (TOA) shortwave radiative cooling over the extratropics (45°N - 65°N) in two different land regions as shown in Figure 2.1.2: North Asia (N.Asia) and North America (N.Amer). We decided to call our experiments as DOM-N.Asia and DOM-N.Amer when we use the fully coupled model and as SOM-N.Asia and SOM-N.Amer when we use the slab ocean model.

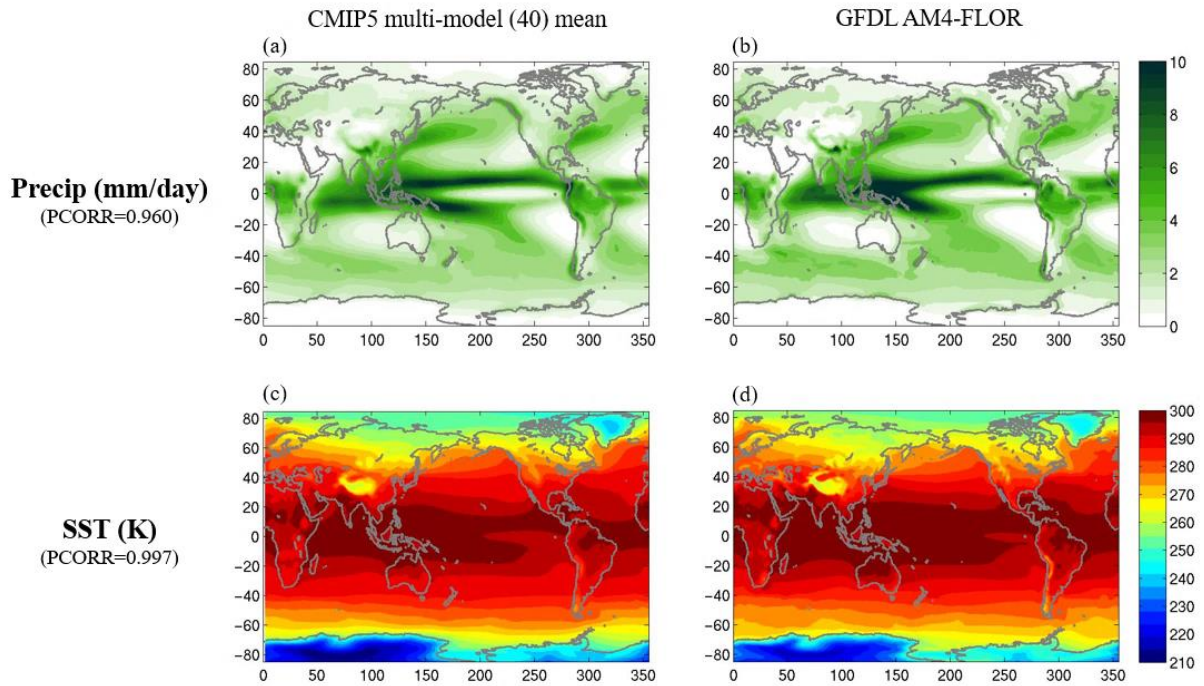


Fig. 2.1.1. Annual mean precipitation (mm/day) and SST (K) from (a, c) the mean of 40 CMIP5 multi-models and (b, d) GFDL AM4-FLOR for pre-industrial control run. PCORR indicates the value of pattern correlation.

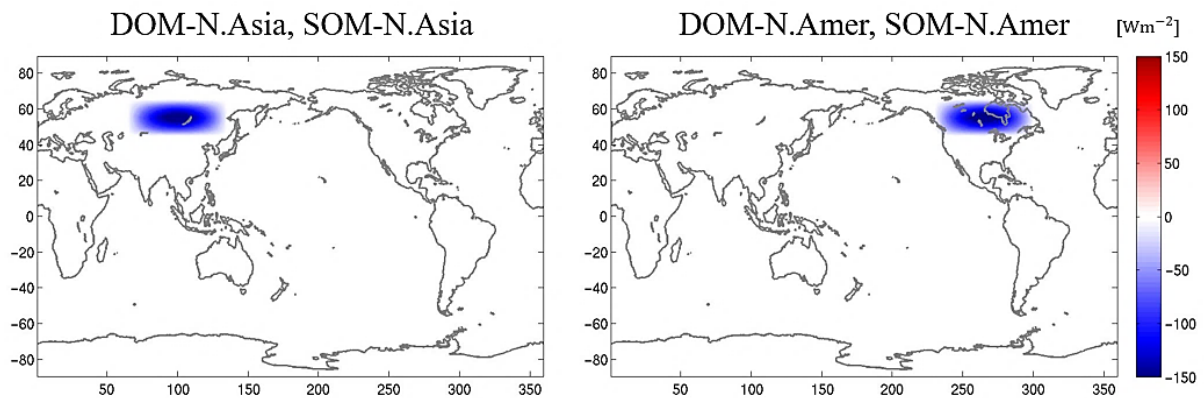


Fig. 2.1.2. Distribution of imposed radiative forcing (Wm^{-2}) over North Asia (left) and North America (right).

In the idealized experiments of previous studies, they found that high-latitude forcing is most effective for the ITCZ shift (Seo et al. 2014). Hence, our experiments inspect the results for high-latitude forcing in the DOM. Moreover, we can expect that the propagation of regional perturbation along the climatological westerly wind will have a significant effect on the adjacent oceans, the Pacific and the Atlantic basins, respectively. In the Pacific, the wind-driven subtropical cells (STCs) and the Ekman flow dominate, while the thermohaline circulation is crucial in the Atlantic. We thus note that the different characteristics of the ocean dynamics in two oceans have diverse influences on tropical climate responses.

All perturbed experiments are integrated for 100 years and the annual-means for the last 70 years are analyzed to avoid the initial transient period. Although 100 years is not enough for the deep overturning ocean circulation to reach an equilibrium state, this period of study provides guidance on potential changes from localized perturbation and enables comparison with previous studies (e.g., Kang et al. 2018). The area-integrated forcing amounts to -0.4 PW in all cases and -1.2 Wm^2 globally averaged. Considering actual global mean radiative forcing due to anthropogenic sulfate is measured to be -0.5 to -1.5 Wm^2 , we concentrate this radiative forcing in each localized region. Given the same magnitude of perturbation by directly reducing the solar constant, we can compare the difference between the perturbations for the same condition. The focus of the analysis is the pattern of response rather than absolute magnitude.

2.2 Analysis Methods

2.2.1 Atmospheric energy budget

The response of the tropical precipitation to the TOA energy perturbations is controlled by the atmospheric energy budget. The imposed radiative perturbation is balanced by changes in the AHT, ocean heat uptake (OHU) and TOA radiation (Kang et al. 2019), as

$$F_{eff} = (1 - \alpha)\langle\Delta S\rangle = \Delta F_{A0} + \langle\Delta Q_{net}\rangle - \langle\Delta R_{TOA}\rangle, \quad (1)$$

where Δ is the change between the perturbed and CTRL runs, S is the insolation, and α is the planetary albedo in CTRL. Brackets denote the spatial integral over the Southern Hemisphere (SH) with the global-mean removed. We consider as F_{eff} the effective forcing term, which is the fraction of insolation perturbation that actually enters the Earth. F_{A0} is the cross-equatorial AHT by integrating the difference between the TOA and surface fluxes from SH to the equator. The OHU response (ΔQ_{net})

is computed as anomalous net downward surface heat flux, and ΔR_{TOA} represents anomalous net downward TOA radiation with the effective forcing term removed. The terms in the equation are calculated as zonally integration and time mean.

We define the three compensations as the fraction of effective forcing balanced by changes in the AHT, OHU, and TOA radiation, respectively, as

$$C_{ATM} \equiv \left| \frac{\Delta F_{A0}}{F_{eff}} \right|, \quad C_{OCN} \equiv \left| \frac{\langle \Delta Q_{net} \rangle}{F_{eff}} \right|, \quad \text{and} \quad C_{TOA} \equiv \left| \frac{\langle \Delta R_{TOA} \rangle}{F_{eff}} \right|, \quad (C_{ATM} + C_{OCN} + C_{TOA} = 1), \quad (2)$$

The degree of compensation for equatorial mean (5°S and 5°N) is used to assess the ITCZ response.

2.2.2 Oceanic energy budget

Based on Liu et al. (2018), we decompose the time mean OHU into two terms:

$$\langle \Delta Q_{net} \rangle = \langle \Delta OHS \rangle + \Delta OHT, \quad (3)$$

where OHS denotes the ocean heat storage and OHT denotes the meridional ocean heat transport. The ocean is a quasi-equilibrium state over our averaging periods, then the change in OHS cannot be zero and is calculated directly as,

$$OHS = \frac{\partial}{\partial t} \iint \rho_0 C_p \theta \, dz \, dx, \quad (4)$$

where x and z are the zonal and vertical coordinates. $\rho_0 = 1027 \, \text{kg m}^{-3}$ is the density of ocean at the sea surface, $C_p = 3985 \, \text{J kg}^{-1} \text{K}^{-1}$ is the heat capacity of ocean, and θ is the ocean potential temperature.

The meridional OHT is separated into four components (Liu et al. 2018; Yang et al. 2015): the Euler mean circulation, the bolus circulation (mesoscale eddies), the sub-mesoscale circulation (induced by eddies on the mixed layer) and the diffusion,

$$\begin{aligned} OHT &= \iint \rho C_p (\bar{v}\theta + v^*\theta + v'\theta + D) \, dz \, dx \\ &= OHT_{Eul} + OHT_{Bol} + OHT_{Sub} + OHT_{Diff}, \quad (5) \end{aligned}$$

where ρ is the ocean density, \bar{v} is the Euler mean meridional velocity, v^* is the bolus velocity, and v' is the sub-mesoscale eddy velocity. D represents the Redi isoneutral diffusion operator (Redi 1982). We output the OHT terms directly except to the diffusion. The diffusion term is then taken as the residual

based on Eqs. (3) and (5). Here we consider a residual term (OHT_{res}) including the bolus, sub-mesoscale circulation and diffusion because the magnitude of the components is relatively much weaker in the tropics,

$$OHT_{res} = OHT_{Bol} + OHT_{Sub} + OHT_{Diff}. \quad (6)$$

Therefore, Eq. (3) can be rewritten as

$$\langle \Delta Q_{net} \rangle = \langle \Delta OHS \rangle + \Delta OHT_{Eul} + \Delta OHT_{res}, \quad (7)$$

which indicates that the response of OHU is determined by changes in the heat storage of ocean and ocean heat transport by Eulerian mean and residual circulations.

2.2.3 Ocean meridional overturning circulation (MOC)

The Euler mean ocean MOC is calculated by integrating Euler mean meridional velocity (\bar{v}) multiplied by water density (ρ) zonally and vertically:

$$\psi_{Eul} = \iint_z^0 \rho \bar{v} dz dx, \quad (8)$$

where z is the vertical coordinate.

III. Results

3.1 Responses of surface temperature and precipitation

In response to the similar magnitude of localized forcing, we analyze the pattern of the results focusing on tropical precipitation and energetics. Figure 3.1.1 shows the global surface temperature response for each experiment. Black outlined boxes indicate each forcing region. All experiments present overall cooling anomalies, even outside the perturbation region, and cool more in the Northern Hemisphere (NH) relative to the SH. The global mean surface temperature response is much cooler in SOM with -0.67 K than in DOM with -0.46 K. This is due to the damping of the cooling response in DOM as the fully coupled model can transfer heat more effectively than the atmosphere alone. Moreover, the warming pattern in the North Atlantic is correlated to the sinking region of the thermohaline circulation and the strengthening of the AMOC in DOM (Delworth et al. 1993). As a consequence, there is a larger hemispheric temperature asymmetry in SOM, which can be readily seen in the zonal-mean (Fig. 3.1.2a).

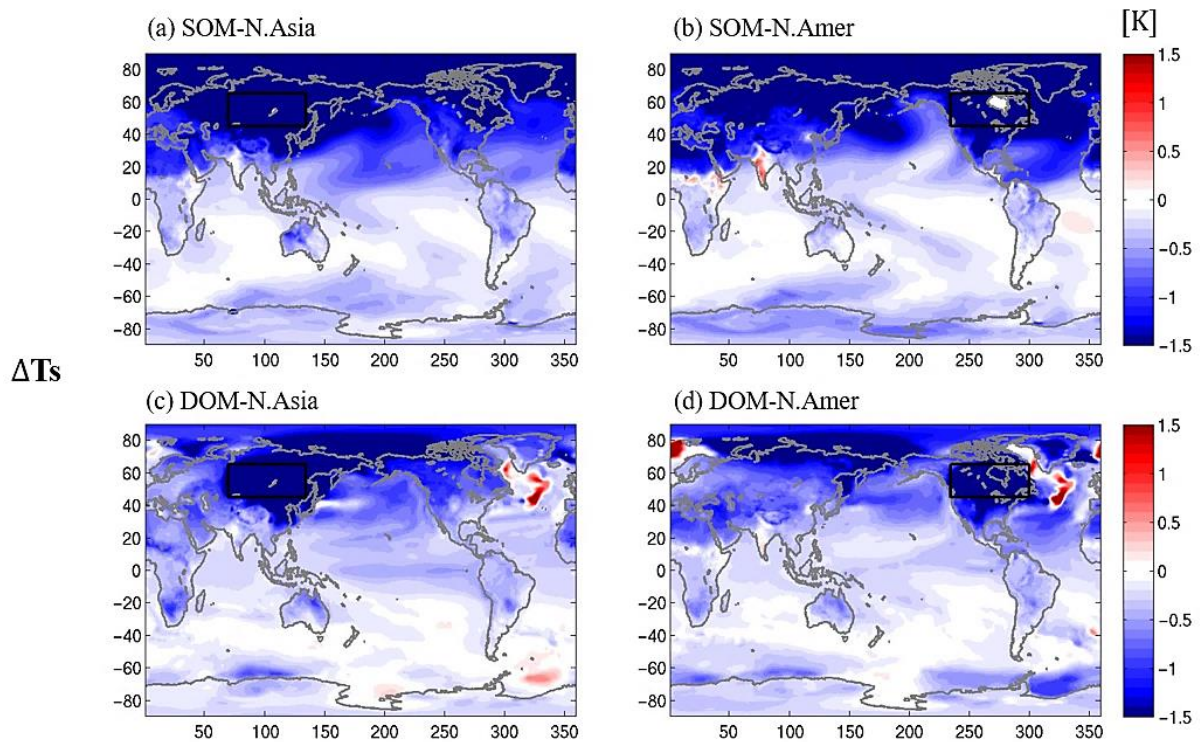


Fig. 3.1.1. The response of annual mean global surface temperature for (a) SOM-N.Asia, (b) SOM-N.Amer, (c) DOM-N.Asia, and (d) DOM-N.Amer. The black outlined boxes indicate the region with the prescribed forcing.

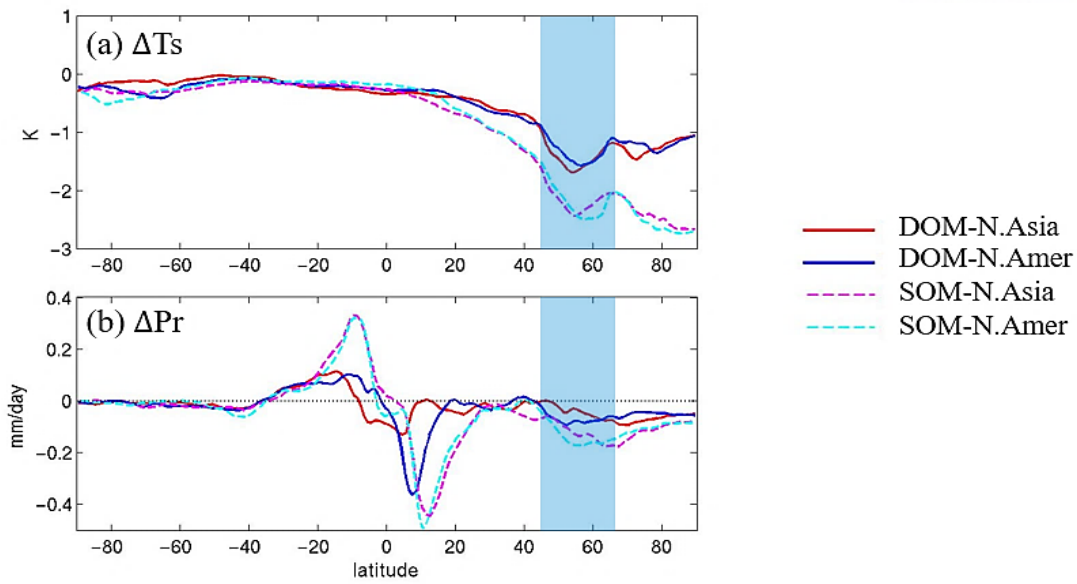


Fig. 3.1.2. The zonal mean responses of (a) surface temperature (K) and (b) precipitation (mm/day) for DOM cases (solid) and SOM cases (dashed). The blue shading regions indicate latitudinal bands of forcing.

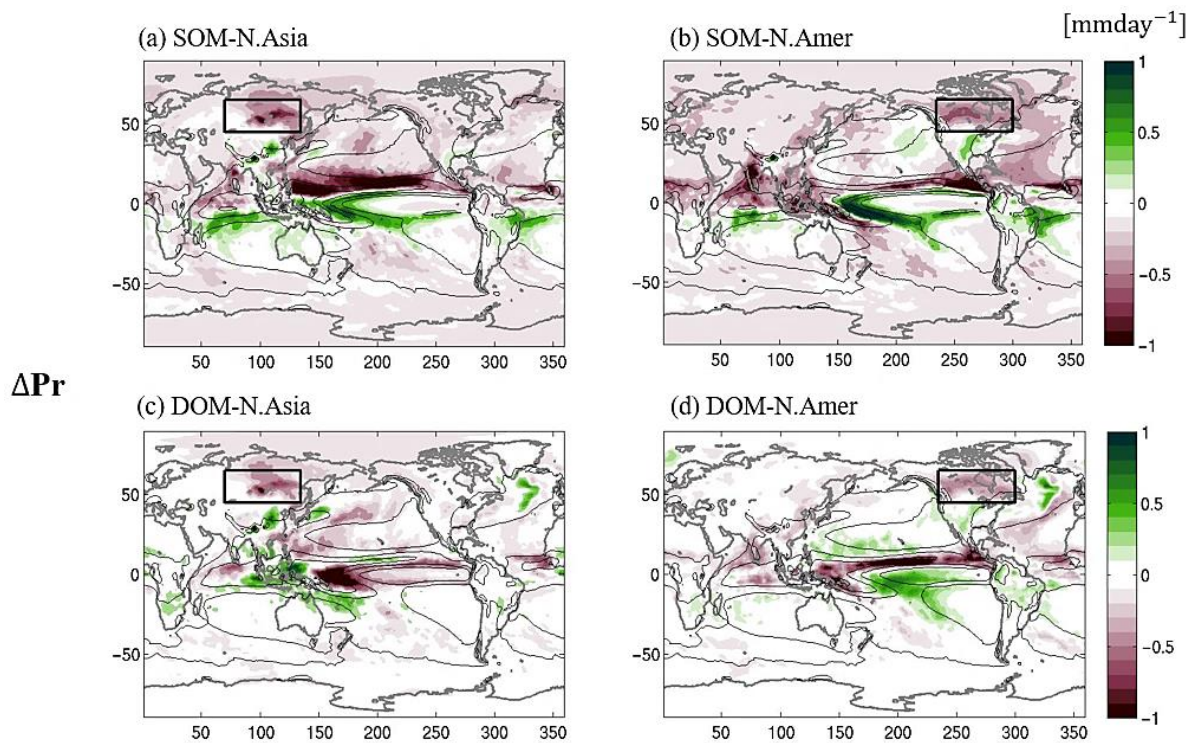


Fig. 3.1.3. The response of annual mean global precipitation (shading) for (a) SOM-N.Asia, (b) SOM-N.Amer, (c) DOM-N.Asia, and (d) DOM-N.Amer. Contours denote the climatological precipitation in the CTRL (contour interval = 3 mm/day). The black outlined boxes indicate the region with the prescribed forcing.

This asymmetry is more effective in making a common southward shift of the ITCZ in SOM (Figs. 3.1.2b, 3.1.3a,b). The results are independent of the forcing location, consistent with previous studies. With the ocean dynamics, however, the precipitation responses are also muted as the surface temperature changes, and the tropical precipitation responses vary depending on the location of the forcing (Figs. 3.1.2b, 3.1.3c,d). In particular, the change of tropical Pacific rainfall pattern in DOM-N.Amer still shows southward shift, but in DOM-N.Asia, there is an equatorial symmetric pattern of tropical precipitation with decreasing over the tropical Pacific Ocean and increasing over the maritime continent. It appears that the climatological maximum rainfall region has moved westward.

3.2 Atmospheric energy budget and TOA radiation response

To find out why tropical precipitation patterns differ, we apply the atmospheric energy budget using equation (1). According to (2), Figure 3.2.1 shows a bar graph of the equatorial mean (5°S to 5°N) fractional compensations of atmospheric, oceanic, and TOA radiation responses for all experiments. C_{ATM} is a fraction of cross-equatorial atmospheric energy transport, which is related to Hadley cell. If we understand C_{ATM} , we can know the ITCZ response.

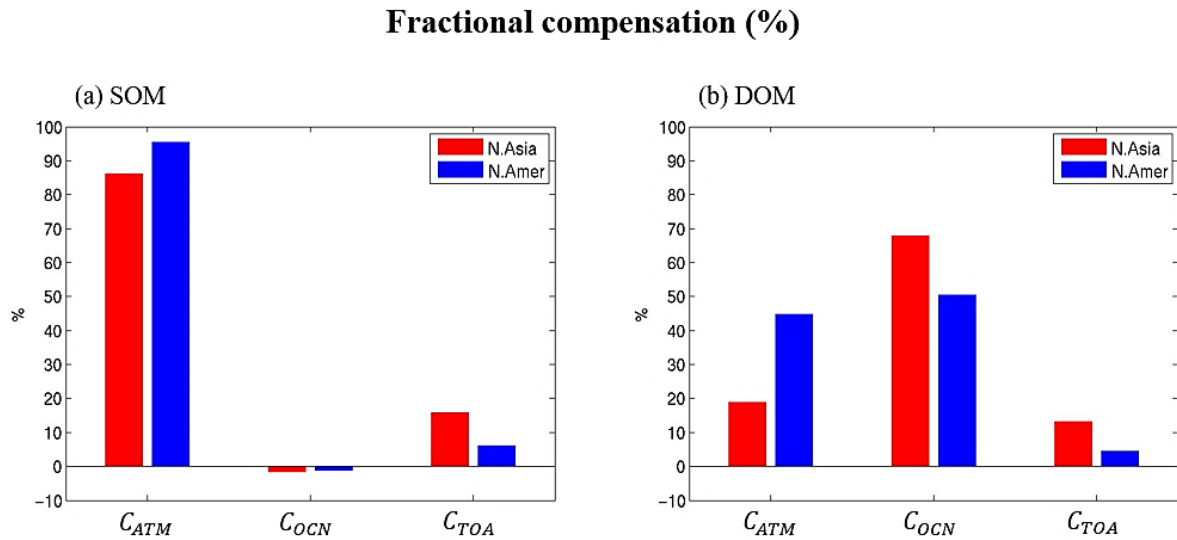


Fig. 3.2.1. The fractional compensation (%) by the atmospheric heat transport (C_{ATM}), the ocean heat uptake (C_{OCN}), and the TOA radiation (C_{TOA}) averaged between 5°S and 5°N for (a) SOM and (b) DOM. The red bar indicates N.Asia case and the blue bar indicates N.Amer case.

Because there is no ocean activity in SOM, the atmosphere compensates most of the forcing with 86% for SOM-N.Asia and with 95% for SOM-N.Amer (Fig. 3.2.1a). This is evident that a clear ITCZ shift is associated with large cross-equatorial anomalous AHT. On the other hand, a relatively smaller C_{ATM} (19% for DOM-N.Asia and 45% for DOM-N.Amer) is linked to a larger C_{OCN} (68% for DOM-N.Asia and 51% for DOM-N.Amer) in DOM (Fig. 3.2.1b). Then C_{TOA} has an almost similar fraction in both SOM and DOM. The changes of C_{ATM} are determined by changes of C_{OCN} or C_{TOA} , so we need to investigate these two terms.

Despite the difference in surface temperature response between SOM and DOM, C_{TOA} has an almost similar ratio in both SOM (16% for SOM-N.Asia and 6% for SOM-N.Amer) and DOM (13% for DOM-N.Asia and 5% for DOM-N.Amer). From the SOM simulations, ΔR_{TOA} tends to show a downward radiation anomaly above the 30°N and upward radiation anomaly in the northern subtropics (10-30°N) in both experiments (Figs. 3.2.2a-c). The downward (upward) radiation anomaly means that the Earth emits less (more) radiation out of the atmosphere, thereby a negative (positive) feedback works to weaken (amplify) the extratropical radiative forcing. The negative feedback occurs mainly as the outgoing longwave radiation (OLR) decreases at the surface in response to the cooling anomaly of the surface temperature above the 30°N. Conversely, increased OLR in the northern subtropics is due to the decrease in the high cloud amount responding to the ITCZ shift. In addition, lower temperature brings higher static stability of the atmosphere and thus increases the amount of low clouds, which in turn enhances the reflection of shortwave radiation, leading to positive feedback. From the DOM simulations (Figs. 3.2.2d-f), the magnitude of the overall ΔR_{TOA} is smaller than the SOM because the atmospheric climate response, such as the changes of ITCZ shift, surface temperature and the amount of cloud, is damped owing to the ocean dynamics. This mostly causes negative feedback in the patterns of zonal mean response in DOM. In other words, in the SOM, the positive feedback in the northern subtropics partially cancels out negative feedback at mid-high latitudes, resulting in similar compensation by TOA radiation like DOM.

The reason why N.Asia is larger than N.Amer in C_{TOA} can be seen in the forcing region over 40-60°N (Fig. 3.2.2). In this latitudinal band, there is generally the negative feedback of TOA radiation. However, this feedback can be offset by the positive feedback from the increased low cloud amount around North America in N.Amer. In contrast, the topographical features of the Gobi Desert and the Tibetan Plateau make strong negative feedback near the forcing region of N.Asia. These regions have very little climatological water vapor, so there is almost no cloud effect. Therefore, with the opposite radiation feedback over the forcing regions of the two experiments, N.Asia is larger in compensation by TOA radiation.

ΔR_{TOA}

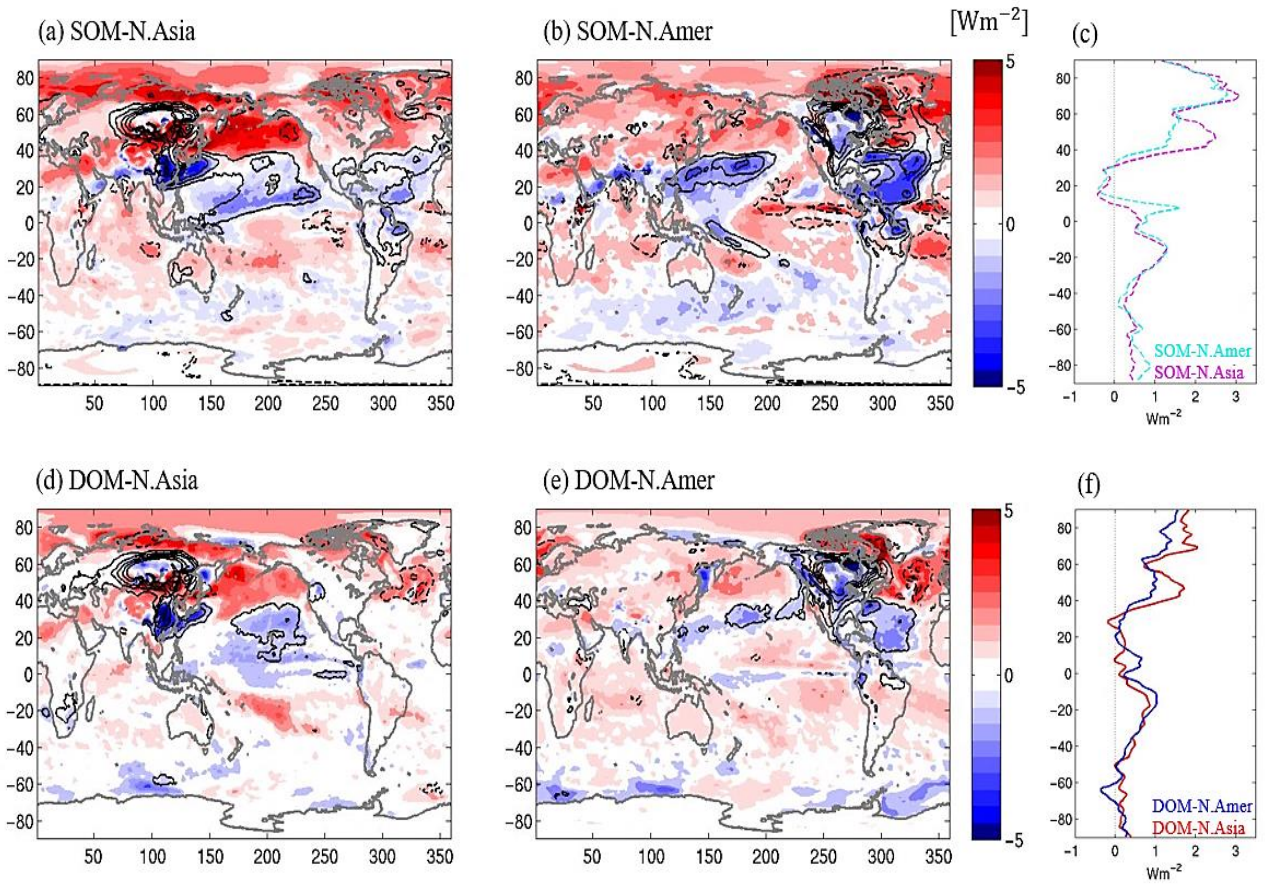


Fig. 3.2.2. The response of TOA radiation (shading; Wm^{-2}) and their zonal-mean plots for (a-c) SOM and (d-f) DOM. Contour indicates the low cloud amount response (in %; positive in solid and negative in dashed). Positive denotes downward fluxes for TOA.

3.3 Ocean heat budget and MOC response

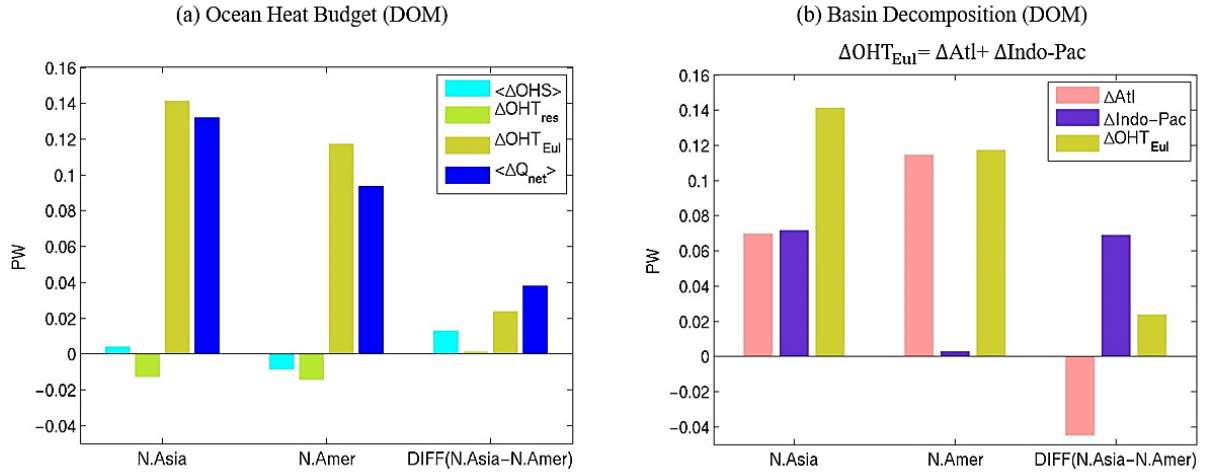


Fig. 3.3.1. (a) Changes of net downward surface heat flux averaged between $5^{\circ}S$ and $5^{\circ}N$ in the total (blue), Eulerian mean OHT (olive), residual OHT (green), and OHS (cyan). (b) The responses of meridional OHT averaged between $5^{\circ}S$ and $5^{\circ}N$ in the total (olive), the Atlantic Ocean (pink), and the Indo-Pacific Ocean (purple).

Because the fractional compensations of TOA radiation are similar, the C_{OCN} eventually determines C_{ATM} changes in DOM. To figure out what decides the energy partitioning response between the atmosphere and ocean, we analyze C_{OCN} using the ocean heat budget in DOM. Figure 3.3.1a shows a bar graph of $\langle \Delta Q_{net} \rangle$ divided by heat storage and heat transport terms using (7). The ocean is the quasi-equilibrium state over our averaging periods, and then there is a small quantity of $\langle \Delta OHS \rangle$ with opposite sign between two experiments. It explains about 30% of the experimental difference (DIFF). According to (5) and (6), OHT terms can be divided into Eulerian mean and residual terms including eddies and diffusion. ΔOHT_{res} acts in the opposite direction to $\langle \Delta Q_{net} \rangle$ and is not taken into account to determine the experimental difference of $\langle \Delta Q_{net} \rangle$ because both experiments have similar values of around -0.01 PW. The dominant factor that determines $\langle \Delta Q_{net} \rangle$ is ΔOHT_{Eul} , which is responsible for the northward heat transport and accounts for about 63% of the experimental differences.

We then decompose the ocean basin into the Atlantic and the Indo-Pacific Ocean using an ocean mask to discuss which ocean circulation is more important to ΔOHT_{Eul} (Fig. 3.3.1b). This bar graph analyzes the equatorial mean values, hence oceans other than the Atlantic and the Indo-Pacific Ocean do not need to be considered. DOM-N.Asia has almost the same proportions of energy transport in both oceans,

but in DOM-N.Amer the Atlantic explains most of $\Delta\text{OHT}_{\text{Eul}}$. The experimental difference in the Indo-Pacific Ocean dominates the total difference.

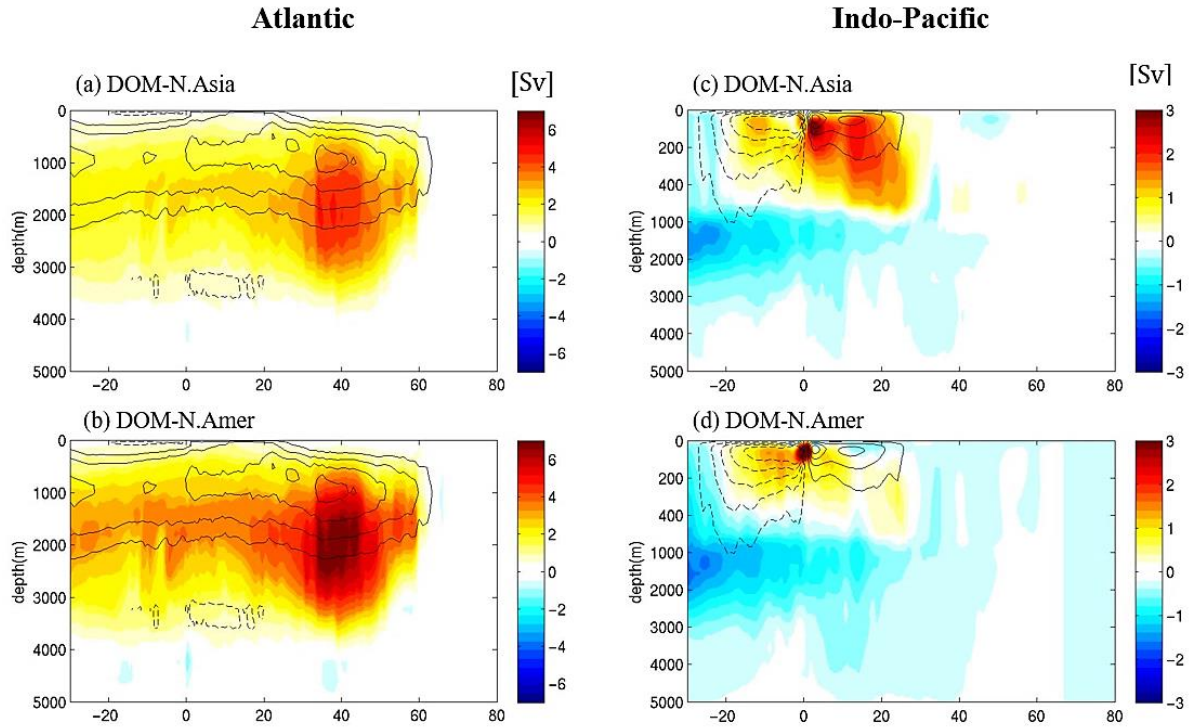


Fig. 3.3.2. The annual mean ocean MOC streamfunction responses (shading; in Sv) and mean ocean MOC in DOM-CTRL (contour interval = 5 Sv) in (a, b) the Atlantic Ocean and (c, d) the Indo-Pacific Ocean. Solid (dashed) contour denotes a clockwise (counterclockwise) circulation.

The ΔOHT in the Atlantic is strongly connected to AMOC, which can also be seen in the mass transport streamfunction anomalies shown in Figure 3.3.2a,b. In both experiments, AMOC is enhanced for extratropical NH cooling, and the strengthening of AMOC leads to a decreased meridional SST gradient in the NH. The maximum AMOC strength is about 5 Sv ($1 \text{ Sv} \equiv 10^6 \text{ m}^3 \text{ s}^{-1}$) for DOM-N.Asia and about 7 Sv for DOM-N.Amer. The strong strength of AMOC in DOM-N.Amer is associated with the forcing domain, which is very close to the AMOC subduction region. The climatological westerly wind at these latitudes induces a cold advection to extratropical forcing and then results in a stronger cooling SST response in the North Atlantic Ocean. It creates these surface waters to become dense and salt, thereby supporting the AMOC subduction, hence, leading to the strengthened AMOC.

Shallow overturning cells in the Pacific Ocean are characterized (Figs. 3.3.2c,d), known as the

subtropical cells (STCs) (McCreary and Lu 1994). The STCs are important for transporting energy with the poleward flow at the ocean surface, subsidence in the subtropics, equatorward return flow, and upwelling in the tropics. The strengthening of the NH STC in DOM-N.Asia is a major contributor in determining the difference in C_{OCN} between the two experiments, carrying a quantity similar to the energy transported by AMOC.

3.4 Coupling of the atmosphere and ocean circulations

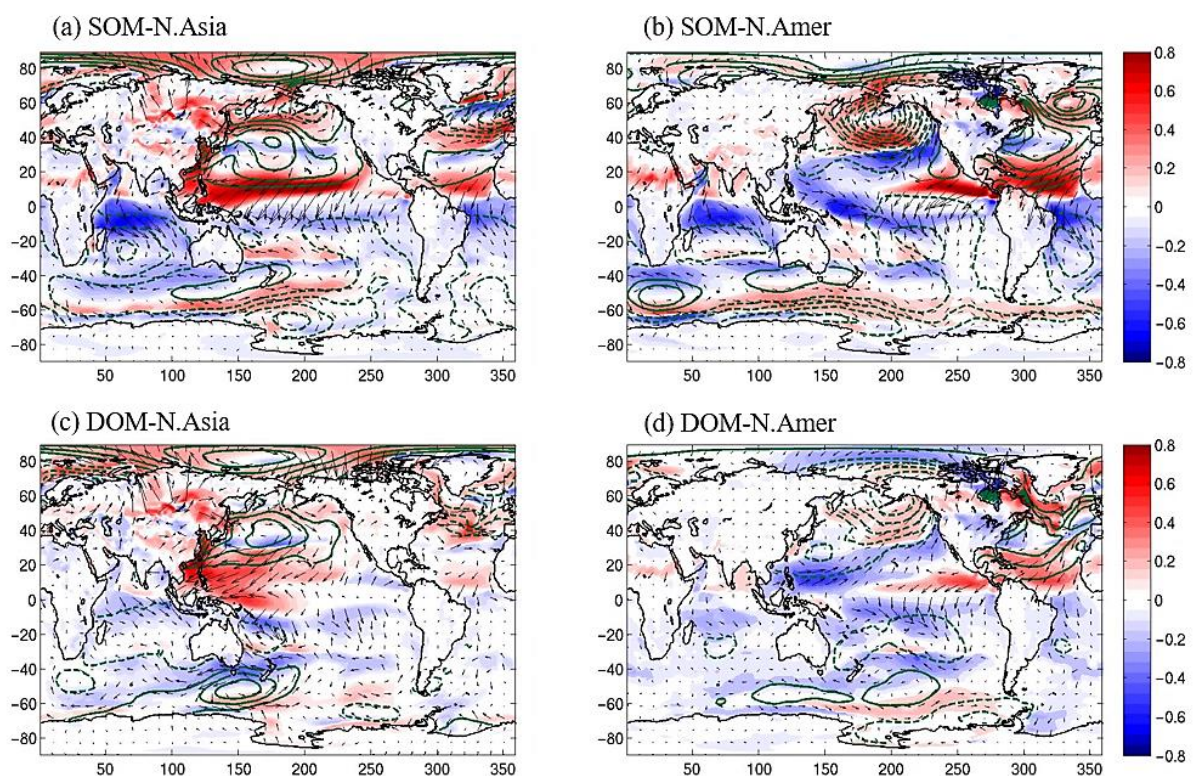


Fig. 3.4.1. Composite annual mean anomalies of surface winds and sea level pressure for (a) SOM-N.Asia, (b) SOM-N.Amer, (c) DOM-N.Asia, and (d) DOM-N.Amer. The shading indicates the wind speed responses. The green contour indicates the sea level pressure responses (contour interval = 0.25 hPa). Solid (dashed) contour denotes the high (low) pressure anomaly. The vectors indicate the 10m wind anomalies.

The reason for the STC change can be found in the change in pressure on the extratropical forcing and the resulting wind response (Fig. 3.4.1). In Hoskins and Karoly (1981), a heat source (Q) in the extratropics is balanced by meridional motion (i.e., $Q \cong -v$). In this experiment, an anomalous cooling ($Q < 0$) is balanced by poleward meridional motion ($v > 0$), which leads to warm advection in the NH.

Thus, it follows that the pressure trough must be to the west of the source region. As a result, a high and low pressure are settled over the North Pacific Ocean and the North Atlantic Ocean, respectively in N.Asia, and N.Amer case is in complete contrast. These pressure patterns are remarkably similar between SOM and DOM, and then the resulting wind responses are comparable with the pattern, except in the equatorial Pacific.

In SOM, the anomalously southward meridional wind over the equatorial Pacific (Figs. 3.4.1a,b) is owing to the strong shift of the ITCZ to the south, as distinct from DOM. High pressure over the North Pacific in DOM-N.Asia induces increasing easterly wind response in the tropical and subtropical North Pacific Ocean (Fig. 3.4.1c). It leads to stronger northward Ekman transport and then NH STC becomes stronger. In DOM-N.Amer, on the contrary, Pacific trade winds tend to be weakened in response to the low-pressure system (Fig. 3.4.1d), hence the influence of Indo-Pacific OHT is very small (Figs. 3.3.1b, 3.3.2d).

In addition, the easterly wind anomaly in DOM-N.Asia is amplified by equatorial upwelling in the eastern Pacific Ocean and a Bjerknes positive feedback (Bjerknes 1969) with a La Nina-like cooling pattern as shown in Figure 3.1.1c. It then strengthens the zonal SST gradient and coupled atmospheric overturning circulation across the equatorial Pacific Ocean. Hence, it changes the tropical precipitation pattern by westward shifting of the Walker circulation upward branch so that it makes the equatorial symmetric pattern of precipitation anomaly (Fig. 3.1.3c). The Atlantic cooling in N.Amer increases the sea level pressure, leading anomalous northeasterly wind across the Central America Isthmus (Figs. 3.4.1b,d) (Xie et al. 2008). It contributes to a weak anomalous SST cooling over the eastern Pacific (Figs. 3.1.1b,d) but it is not effective enough to trigger strong feedback.

IV. Conclusion and Discussion

This study examines the sensitivity of the pattern of tropical precipitation response resulting from the radiative forcing over different continents. Radiative cooling is prescribed over extratropical North Asia (N.Asia) and extratropical North America (N.Amer) in both SOM and DOM (Fig. 2.1.2). The simulations are set to cool the NH, thereby inducing a southward ITCZ shift. We focus on how the components of the energy budget modulate the tropical response to semi-idealized radiative perturbation.

The tropical responses in the SOM experiments share the common precipitation response pattern, which is shaped by the southward ITCZ shift (Fig. 3.1.3a,b). Because there is no ocean dynamics in the SOM, the atmospheric heat transport accounts for most of the forcing compensation (Fig. 3.2.1a). The strong interhemispheric temperature asymmetry (Fig. 3.1.2a) induces the change of Hadley circulation, atmospheric heat transport, and ITCZ position. Without ocean dynamics, the tropical response patterns are insensitive to the zonally asymmetric perturbation in the extratropics, consistent with previous studies using the slab ocean model.

Compared with SOM responses, the DOM experiments produce different pattern distribution of precipitation responses depending on the extratropical localized forcing: DOM-N.Amer shows a southward shift of tropical precipitation pattern, whereas DOM-N.Asia shows a westward shift of tropical precipitation patterns (Fig. 3.1.3c,d). This difference of patterns is determined by the anomalous pressure over the Northern Pacific Ocean and the resulting wind response (Fig. 3.4.1c,d). In DOM-N.Asia, the anomalous high pressure located in the Northern Pacific Ocean strengthens the northeasterly over the tropical Pacific Ocean. The wind response is coupled with wind-driven circulation, making stronger NH STC (Fig. 3.3.2c) and northward OHT in the Indo-Pacific Ocean (Fig. 3.3.1b). It is important in the equatorial symmetric pattern formation of tropical precipitation response through a westward shift of the Walker circulation upward branch in response to interactions of atmosphere-ocean coupling. On the other hand, in DOM-N.Amer, the STC or Indo-Pacific OHT cannot be strongly affected owing to the low-pressure anomaly located in the Northern Pacific Ocean, which rather weakens the trade winds (Fig. 3.4.1d). Instead, the strong cooling over the Northern Atlantic Ocean accelerates the AMOC (Fig. 3.3.2b), responsible for ocean compensation in DOM-N.Amer (Fig. 3.3.1b). As a result, DOM-N.Amer represents the southward ITCZ shift like SOM, having a damping response.

Although these experiments use semi-idealized perturbation, from the industrial period we have experienced local variations of radiative forcing due to aerosol distribution. Aerosols generally lead to

a net cooling effect by reducing the radiation reaching the surface in such a way that the aerosols reflect incoming solar radiation and interact with clouds, resulting in southward ITCZ shift (Rotstayn and Lohmann 2002; Ridley et al. 2015; Hwang et al. 2013; Voigt et al. 2017; Allen and Ajoku 2016). Global emissions of anthropogenic aerosols peaked in the 1970s over the United States and Europe, and their aerosol emissions are decreasing due to the clean air regulations (Klimont et al. 2013; Smith et al. 2011; Smith and Bond 2014; Leibensperger et al. 2012; Tørseth et al. 2012). In contrast, the contribution of Asia has been rapidly increasing in the past couple of decades (Klimont et al. 2013; Li et al. 2017; Lu et al. 2011). It means that the major contributor has shifted from Euro-North America to Asia, then this will have implications for the forcing location in our simulations. We will also extend this study, suggesting the decomposition of average and difference between N.Asia and N.Amer, and the comparison between the average and run of zonally uniform forcing in ETIN-MIP (Kang et al. 2019). It would be informative to figure out what produces the observed historical pattern of La Nina-like SST in the equatorial Pacific to various radiative forcing.

References

- Allen, R. J., & Ajoku, O. (2016). Future aerosol reductions and widening of the northern tropical belt. *Journal of Geophysical Research: Atmospheres*, *121*(12), 6765-6786.
- Allen, R. J., Evan, A. T., & Booth, B. B. (2015). Interhemispheric aerosol radiative forcing and tropical precipitation shifts during the late twentieth century. *Journal of Climate*, *28*(20), 8219-8246.
- Bjerknes, J. (1969). Atmospheric teleconnections from the equatorial Pacific. *Monthly weather review*, *97*(3), 163-172.
- Ceppi, P., Hwang, Y. T., Liu, X., Frierson, D. M., & Hartmann, D. L. (2013). The relationship between the ITCZ and the Southern Hemispheric eddy-driven jet. *Journal of Geophysical Research: Atmospheres*, *118*(11), 5136-5146.
- Chiang, J. C., & Bitz, C. M. (2005). Influence of high latitude ice cover on the marine Intertropical Convergence Zone. *Climate Dynamics*, *25*(5), 477-496.
- Delworth, T., Manabe, S., & Stouffer, R. J. (1993). Interdecadal variations of the thermohaline circulation in a coupled ocean-atmosphere model. *Journal of Climate*, *6*(11), 1993-2011.
- Deser, C., Tomas, R. A., & Sun, L. (2015). The role of ocean-atmosphere coupling in the zonal-mean atmospheric response to Arctic sea ice loss. *Journal of Climate*, *28*(6), 2168-2186.
- Feddema, J. J., Oleson, K. W., Bonan, G. B., Mearns, L. O., Buja, L. E., Meehl, G. A., & Washington, W. M. (2005). The importance of land-cover change in simulating future climates. *Science*, *310*(5754), 1674-1678.
- Frierson, D. M., Hwang, Y. T., Fučkar, N. S., Seager, R., Kang, S. M., Donohoe, A., ... & Battisti, D. S. (2013). Contribution of ocean overturning circulation to tropical rainfall peak in the Northern Hemisphere. *Nature Geoscience*, *6*(11), 940.
- Fučkar, N. S., Xie, S. P., Farneti, R., Maroon, E. A., & Frierson, D. M. (2013). Influence of the extratropical ocean circulation on the intertropical convergence zone in an idealized coupled general circulation model. *Journal of Climate*, *26*(13), 4612-4629.
- Green, B., & Marshall, J. (2017). Coupling of trade winds with ocean circulation damps ITCZ shifts. *Journal of Climate*, *30*(12), 4395-4411.
- Hawcroft, M., Haywood, J. M., Collins, M., & Jones, A. (2018). The contrasting climate response to tropical and extratropical energy perturbations. *Climate dynamics*, *51*(9-10), 3231-3249.
- Hawcroft, M., Haywood, J. M., Collins, M., Jones, A., Jones, A. C., & Stephens, G. (2017). Southern Ocean albedo, inter-hemispheric energy transports and the double ITCZ: Global impacts of biases in a coupled model. *Climate Dynamics*, *48*(7-8), 2279-2295.
- Hoskins, B. J., & Karoly, D. J. (1981). The steady linear response of a spherical atmosphere to thermal and orographic forcing. *Journal of the Atmospheric Sciences*, *38*(6), 1179-1196.
- Hwang, Y. T., Frierson, D. M., & Kang, S. M. (2013). Anthropogenic sulfate aerosol and the southward shift of tropical precipitation in the late 20th century. *Geophysical Research Letters*, *40*(11), 2845-2850.
- Kang, S. M., Hawcroft, M., Xiang, B., Hwang, Y. T., Cazes, G., Codron, F., ... & Kim, J. (2019). ETIN-MIP Extratropical-Tropical Interaction Model Intercomparison Project-Protocol and Initial

Results. *Bulletin of the American Meteorological Society*, (2019).

Kang, S. M., Held, I. M., Frierson, D. M., & Zhao, M. (2008). The response of the ITCZ to extratropical thermal forcing: Idealized slab-ocean experiments with a GCM. *Journal of Climate*, 21(14), 3521-3532.

Kang, S. M., Park, K., Hwang, Y. T., & Hsiao, W. T. (2018). Contrasting tropical climate response pattern to localized thermal forcing over different ocean basins. *Geophysical Research Letters*, 45(22), 12-544.

Kang, S. M., Shin, Y., & Xie, S. P. (2018). Extratropical forcing and tropical rainfall distribution: energetics framework and ocean Ekman advection. *npj Climate and Atmospheric Science*, 1(1), 1-10.

Kay, J. E., Wall, C., Yettella, V., Medeiros, B., Hannay, C., Caldwell, P., & Bitz, C. (2016). Global climate impacts of fixing the Southern Ocean shortwave radiation bias in the Community Earth System Model (CESM). *Journal of Climate*, 29(12), 4617-4636.

Klimont, Z., Smith, S. J., & Cofala, J. (2013). The last decade of global anthropogenic sulfur dioxide: 2000–2011 emissions. *Environmental Research Letters*, 8(1), 014003.

Leibensperger, E. M., Mickley, L. J., Jacob, D. J., Chen, W. T., Seinfeld, J. H., Nenes, A., ... & Rind, D. (2012). Climatic effects of 1950–2050 changes in US anthropogenic aerosols—Part 2: Climate response. *Atmospheric Chemistry and Physics*, 12(7), 3349-3362.

Levis, S., Bonan, G. B., & Bonfils, C. (2004). Soil feedback drives the mid-Holocene North African monsoon northward in fully coupled CCSM2 simulations with a dynamic vegetation model. *Climate Dynamics*, 23(7-8), 791-802.

Li, H., Zhang, Q., Zhang, Q., Chen, C., Wang, L., Wei, Z., ... & Prévôt, A. S. (2017). Wintertime aerosol chemistry and haze evolution in an extremely polluted city of the North China Plain: significant contribution from coal and biomass combustion. *Atmospheric Chemistry and Physics*, 17(7), 4751-4768.

Liu, W., Lu, J., Xie, S. P., & Fedorov, A. (2018). Southern Ocean heat uptake, redistribution, and storage in a warming climate: The role of meridional overturning circulation. *Journal of Climate*, 31(12), 4727-4743.

Lu, Z., Zhang, Q., & Streets, D. G. (2011). Sulfur dioxide and primary carbonaceous aerosol emissions in China and India, 1996–2010. *Atmospheric Chemistry and Physics*, 11(18), 9839-9864.

Matthews, H. D., Weaver, A. J., Meissner, K. J., Gillett, N. P., & Eby, M. (2004). Natural and anthropogenic climate change: incorporating historical land cover change, vegetation dynamics and the global carbon cycle. *Climate Dynamics*, 22(5), 461-479.

McCreary Jr, J. P., & Lu, P. (1994). Interaction between the subtropical and equatorial ocean circulations: The subtropical cell. *Journal of Physical Oceanography*, 24(2), 466-497.

Merlis, T. M., Zhao, M., & Held, I. M. (2013). The sensitivity of hurricane frequency to ITCZ changes and radiatively forced warming in aquaplanet simulations. *Geophysical Research Letters*, 40(15), 4109-4114.

Notaro, M., Vavrus, S., & Liu, Z. (2007). Global vegetation and climate change due to future increases in CO₂ as projected by a fully coupled model with dynamic vegetation. *Journal of Climate*, 20(1), 70-90.

- Redi, M. H. (1982). Oceanic isopycnal mixing by coordinate rotation. *Journal of Physical Oceanography*, 12(10), 1154-1158.
- Ridley, H. E., Asmerom, Y., Baldini, J. U., Breitenbach, S. F., Aquino, V. V., Pruffer, K. M., ... & Zhang, M. (2015). Aerosol forcing of the position of the intertropical convergence zone since AD 1550. *Nature Geoscience*, 8(3), 195.
- Rotstayn, L. D., & Lohmann, U. (2002). Tropical rainfall trends and the indirect aerosol effect. *Journal of Climate*, 15(15), 2103-2116.
- Schneider, T. (2017). Feedback of Atmosphere-Ocean Coupling on Shifts of the Intertropical Convergence Zone. *Geophysical Research Letters*, 44(22), 11-644.
- Schneider, T., Bischoff, T., & Haug, G. H. (2014). Migrations and dynamics of the intertropical convergence zone. *Nature*, 513(7516), 45-53.
- Seo, J., Kang, S. M., & Frierson, D. M. (2014). Sensitivity of intertropical convergence zone movement to the latitudinal position of thermal forcing. *Journal of Climate*, 27(8), 3035-3042.
- Sewall, J. O., & Sloan, L. C. (2004). Disappearing Arctic sea ice reduces available water in the American west. *Geophysical Research Letters*, 31(6).
- Smith, S. J., & Bond, T. C. (2014). Two hundred fifty years of aerosols and climate: the end of the age of aerosols. *Atmospheric Chemistry and Physics*, 14(2), 537-549.
- Smith, T. E. L., Wooster, M. J., Tattaris, M., & Griffith, D. W. T. (2011). Absolute accuracy and sensitivity analysis of OP-FTIR retrievals of CO₂, CH₄ and CO over concentrations representative of "clean air" and "polluted plumes". *Atmospheric Measurement Techniques*, 4(1), 97-116.
- Tørseth, K., Aas, W., Breivik, K., Fjærraa, A. M., Fiebig, M., Hjellbrekke, A. G., ... & Yttri, K. E. (2012). Introduction to the European Monitoring and Evaluation Programme (EMEP) and observed atmospheric composition change during 1972–2009. *Atmospheric Chemistry and Physics*, 12(12), 5447-5481.
- Vecchi, G. A., Delworth, T., Gudgel, R., Kapnick, S., Rosati, A., Wittenberg, A. T., ... & Jia, L. (2014). On the seasonal forecasting of regional tropical cyclone activity. *Journal of Climate*, 27(21), 7994-8016.
- Voigt, A., Pincus, R., Stevens, B., Bony, S., Boucher, O., Bellouin, N., ... & Zhang, H. (2017). Fast and slow shifts of the zonal-mean intertropical convergence zone in response to an idealized anthropogenic aerosol. *Journal of Advances in Modeling Earth Systems*, 9(2), 870-892.
- Voigt, A., Stevens, B., Bader, J., & Mauritsen, T. (2014). Compensation of hemispheric albedo asymmetries by shifts of the ITCZ and tropical clouds. *Journal of Climate*, 27(3), 1029-1045.
- Westervelt, D. M., Conley, A. J., Fiore, A. M., Lamarque, J. F., Shindell, D. T., Previdi, M., ... & Horowitz, L. W. (2018). Connecting regional aerosol emissions reductions to local and remote precipitation responses. *Atmospheric Chemistry and Physics*, 18(16), 12461-12475.
- White, R. H., McFarlane, A. A., Frierson, D. M., Kang, S. M., Shin, Y., & Friedman, M. (2018). Tropical precipitation and cross-equatorial heat transport in response to localized heating: basin and hemisphere dependence. *Geophysical Research Letters*, 45(21), 11-949.
- Xiang, B., Zhao, M., Ming, Y., Yu, W., & Kang, S. M. (2018). Contrasting impacts of radiative forcing in the southern ocean versus southern tropics on ITCZ position and energy transport in one GFDL

climate model. *Journal of Climate*, 31(14), 5609-5628.

Xie, S. P., Okumura, Y., Miyama, T., & Timmermann, A. (2008). Influences of Atlantic climate change on the tropical Pacific via the Central American Isthmus. *Journal of Climate*, 21(15), 3914-3928.

Yang, H., Li, Q., Wang, K., Sun, Y., & Sun, D. (2015). Decomposing the meridional heat transport in the climate system. *Climate Dynamics*, 44(9-10), 2751-2768.

Yu, S., & Pritchard, M. S. (2019). A Strong Role for the AMOC in Partitioning Global Energy Transport and Shifting ITCZ Position in Response to Latitudinally Discrete Solar Forcing in CESM1. 2. *Journal of Climate*, 32(8), 2207-2226.

Zhao, M., Golaz, J. C., Held, I. M., Guo, H., Balaji, V., Benson, R., ... & Dunne, K. (2018). The GFDL global atmosphere and land model AM4. 0/LM4. 0: 1. Simulation characteristics with prescribed SSTs. *Journal of Advances in Modeling Earth Systems*, 10(3), 691-734.